

Cite this: *J. Mater. Chem. B*, 2019,
7, 4973

Amphiphilic polymers based on polyoxazoline as relevant nanovectors for photodynamic therapy†

Amandine Oudin,^{ab} Julie Chauvin,^a Laure Gibot,^{ac} Marie-Pierre Rols,^c
Stéphanie Balor,^d Dominique Goudounèche,^e Bruno Payré,^e Barbara Lonetti,^{id a}
Patricia Vicendo,^a Anne-Françoise Mingotaud^{id *a} and Vincent Lapinte^{id *b}

An amphiphilic polymer (CmPOX) based on poly(2-methyl-2-oxazoline) linked to a hydrophobic part composed of an aliphatic chain ending with a photo-active coumarin group has been synthesized. It exhibits the ability of forming small polymeric self-assemblies, typically of ca. 10 nm in size, which were characterized by TEM, cryo-TEM and DLS. The nanocarriers were further formulated to yield photo-crosslinked systems by dimerization of coumarin units of coumarin-functionalized poly(methyl methacrylate) (CmPMMA) and CmPOX. The formed vectors were used to encapsulate Pheophorbide a, a known photosensitizer for photodynamic therapy. Cytotoxicity as well as phototoxicity experiments performed *in vitro* on human tumor cells revealed the great potential of these nanovectors for photodynamic therapy.

Received 18th January 2019,
Accepted 8th July 2019

DOI: 10.1039/c9tb00118b

rsc.li/materials-b

Introduction

In various scientific fields, medicine included, an external control of the desired process is often looked for. From this standpoint, light is an interesting stimulus, since it can be easily switched on/off, be very localized and can penetrate between micrometers and centimeters of tissue depending on the wavelength used. With the development of a large variety of medical lasers, photomedicine has therefore strongly progressed in the last 30 years. Among the techniques of photomedicine, photodynamic therapy (PDT) is a clinically approved technique using photosensitizers that yields reactive oxygen species (ROS) upon irradiation, followed by cell death. Since irradiation is a typical local stimulus, PDT provides localized treatment, which is highly desirable in many illnesses in dermatology, ophthalmology or

oncology. A limiting step, however, is that the photosensitizer should be specifically distributed in the area to be treated and this is rarely the case after intra-venous injection. Uncontrolled biodistribution leads to an adverse effect, a cutaneous photosensitivity of the patient for several days. Because such an uncontrolled biodistribution of drugs is a central drawback of many treatments, not only for PDT, the last twenty years have seen a burst of studies aiming at developing nanovectors to improve the therapeutic efficiency of known drugs.^{1–3} This was partly legitimized by the discovery of the so called “Enhanced Permeability and Retention” (EPR) effect by Maeda in the late eighties.^{4,5} This phenomenon showed that, owing to the presence of disjunctions between endothelial cells in vessels close to solid tumors and the low efficiency of lymphatic drainage, some nanovectors could be used to carry drugs in a passive targeting manner. A required specification for this passive targeting is that the vectors should travel undetected in the blood stream until they reach the tumor site. Among all nanocarrier surface compositions assessed, poly(ethylene oxide) (PEO) appeared to be the most efficient and is currently the polymer most widely used for nanovectors.

In this context, PDT has also been evaluated using the tools of nanomedicine and more especially polymeric nanovectors.⁶ Various systems have thus been examined, based on polyesters, polyacrylates, polyacrylamides or peptides. . . Our team has formerly described the encapsulation of a photosensitizer, namely Pheophorbide a, in various polymeric micelles and polymersomes,^{7,8} showing *in vitro* an improvement of photosensitizer delivery and antitumoral activity after light irradiation. Interestingly, crosslinked vectors were even more efficient.⁹ Some of the most

^a Laboratoire des IMRCP, Université de Toulouse, CNRS UMR 5623, Université Paul Sabatier, 118 route de Narbonne, F-31062, Toulouse Cedex 9, France.

E-mail: afmingo@chimie.ups-tlse.fr

^b Institut Charles Gerhardt Montpellier UMR5253 CNRS-UM-ENSCM, Equipe Ingénierie et Architectures Macromoléculaires, Université Montpellier – Bat. 17-cc1702, Place Eugène Bataillon, F-34095 Montpellier Cedex 5, France.

E-mail: vincent.lapinte@umontpellier.fr

^c Institut de Pharmacologie et Biologie Structurale, IPBS, Université de Toulouse, CNRS, UPS, Toulouse, France

^d Microscopie Electronique Intégrative, Centre de Biologie Intégrative, 118 Rte de Narbonne, 31062 Toulouse, France

^e Centre de Microscopie Electronique Appliquée à la Biologie, Faculté de Médecine Toulouse Rangueil, Université de Toulouse, 133, route de Narbonne, 31062 Toulouse Cedex 4, France

† Electronic supplementary information (ESI) available: Experimental details and characterization. See DOI: 10.1039/c9tb00118b

recent studies in the literature examined high-performance vectors, compensating the relative hypoxia of tumors.^{10–12} Among all the existing literature on polymeric nanovectors used for PDT, *ca.* 90% is based on PEO hydrophilic blocks, very much like all other nanomedicine applications of nanovectors. Only very scarcely is another type used, such as polysaccharide.^{13–15}

Ten years ago, some studies began to show that PEO might not be the suggested “gold standard”,¹⁶ as revealed by the occurrence of accelerated blood clearance (ABC) upon several injections, and possible immune responses leading to the loss of the EPR effect after a second injection. Over the last ten years, many studies on this point have been published and it is still a subject of debate.^{17–19} This has led to further evaluation of other polymer types, and a promising lead is poly(2-alkyl-2-oxazoline)s (POx).²⁰ Indeed, this family of polymers offers the advantage of exhibiting different hydrophilicities depending on the alkyl group. An excellent recent review by Luxenhofer on poly(2-alkyl-2-oxazoline)s in biomaterials summarized some data on their toxicity, degradability, stealth properties, immunogenicity and biodistribution.²¹ Different POx structures have been examined, such as partially hydrolyzed POx, and random and block copolymers of cationic and non-ionic POx.²² Regarding the accelerated blood clearance and immunogenicity of poly(2-alkyl-2-oxazoline)s, conflicting results have been published. Szoka showed ABC for PEG and POx liposomes,²³ whereas Wyffels and Hoogenboom found another POx-based system to be non-immunogenic.²⁴ Owing to the need of controlling the state of the nanovectors, photostimulation has often been estimated, and this is also true for POx systems, with different examples of grafted chromophores and the most often aim being photocrosslinking for tissue engineering.^{25–27} Interestingly, more than 20 years ago, Saegusa followed by Chujo described the deamidation of poly(2-methyl-oxazoline) followed by grafting of carboxylated-coumarin groups for the formation of gels.^{28,29} Coumarin is a benzopyrone that can be reversibly dimerized upon irradiation.

These biomedical examples using the POx platform demonstrate the possible strength of this class of polymers along with its versatility. It is, however, surprising that among all these studies, only one example so far has assessed POx polymers as a possible platform for PDT nanovectors. In 2010, Lai *et al.* described the synthesis of poly(2-ethyl-2-oxazoline-*b*-D,L-lactide) to encapsulate the photosensitizer *meta*-tetra(hydroxyphenyl)chlorin.³⁰ They did not observe any PDT improvement by encapsulation, emphasized the possible pH-dependent release of the photosensitizer and showed *in vivo* that cutaneous photosensitivity was decreased by the encapsulation.

Based on this lack of examples in the literature, the assessment of POx as a possible photosensitizer nanovector is relevant. We therefore present here poly(2-methyl-2-oxazoline) self-assemblies as a potential Pheophorbide a carrier. Since this polymer is hydrophilic, self-assemblies were generated after chemical modification, introducing an alkyl chain, as reported in a previous example.³¹ To further examine the effect of crosslinking on this type of vector, a coumarin photoreactive group was also introduced. Besides its possible photodimerization, it is also known to exhibit anti-cancer activities and many derivatives

have been produced for this purpose.^{32,33} The use of such a functional moiety in the formulation of a nanovector could thus provide a synergistic effect in PDT.

Furthermore, another originality of our work lies in the use of a coumarin-bearing oligomethacrylate chain to guarantee the photocrosslinking of the entire self-assembly. This concept could also be extended and the oligomethacrylate chain could be used to easily include other functionalities in the cross-linked nanovector.

Materials and methods

4-Methylumbelliferone, 11-bromo-1-undecanol, diethylether, ethanol, acetone, *p*-toluenesulfonyl chloride, piperidine, pyridine, MgSO₄, potassium carbonate (K₂CO₃) and dodecanethiol (DDT) were purchased from Aldrich and used without further purification. 2-Methyl-2-oxazoline (MOXA) and acetonitrile were distilled over CaH₂ just prior to use. Pheophorbide a (Pheo) was obtained from Wako Inc. Coumarin-functionalized methyl methacrylate (CmMMA) and coumarin tosylate were synthesized and purified by recrystallization according to already published protocols³¹ (Fig. S1 and S2, ESI[†]). Acetonitrile and chloroform were distilled over CaH₂ and stored under nitrogen. Ultrapure water was obtained from an ELGA Purelab Flex system (resistivity higher than 18.2 MΩ cm) and was filtered using 0.2 μm RC filters just before use.

Typical cationic ring-opening polymerization of MOXA

The reaction was performed under nitrogen. The coumarin tosylate initiator (0.383 g, 0.78 mmol) and MOXA (1 mL, 11.8 mmol) were dissolved in 4 mL of anhydrous acetonitrile. The solution was stirred at 80 °C for 7 h, followed by the addition of piperidine (0.39 mL, 3.92 mmol) at room temperature followed by 15 h stirring. The polymer was precipitated in cold diethylether (0 °C) and dried under vacuum. The product was obtained with a 69% yield.

CmPOX: ¹H NMR (400 MHz, CDCl₃) (Fig. S2, ESI[†]), δ = 7.4 (d, 1H, H6), 6.8 (d, 1H, H7), 6.7 (s, 1H, H9), 6.1 (s, 1H, H2), 3.9 (m, 2H, H11), 3.7–3.2 (m, (4n + 2)H, Ha), 2.4 (s, 3H, H4), 2.4–2.1 (m, 3n, Hb), 1.8–1.2 (m, 18H, 13–21).

*M*_n, 3140 g mol⁻¹, *M*_w, 3840 g mol⁻¹, *D* 1.22 (Fig. S3, ESI[†]).

Formation of polymer self-assemblies

20 mg of polymer was dissolved in 2.5 mL of water. If needed, a small volume of additive acetone solution (12–15 μL of CmMMA or CmPMMA solution, calculated to have a final desired ratio of either 6 or 13 wt% compared to CmPOX) was added under stirring at room temperature. The solution was left standing for 2 days to evaporate acetone.

Coumarin dimerization

A 5 mm NMR tube containing 2.2 mL of the self-assembly solution was placed for 7 h between two UV lamps (Fig. S4 and S5, ESI[†]), Philips linear T5 8W, irradiation at 360 nm, lamp-tube distance 8 mm, total irradiance 1.0 mW cm⁻², measured using a HD9021 photometer obtained from Delta Ohm Inc.

Polymerization of CmPOX/CmMMA micelles

The procedure was similar to already published procedures.⁹ Typically, the micelle solution as prepared in the previous paragraph (8 mg mL⁻¹) was purged with argon for 20 min and heated at 50 °C for 48 h.

CmMMA telomerization

The telomerization was carried out in acetonitrile using dodecane-thiol as a telogen agent with a DDT/CmMMA ratio of 0.1 mol/mol. CmMMA (2.59 g, 6.25 mmol) and DDT (0.15 mL, 0.625 mmol) were dissolved in 12 mL of acetonitrile and the solution was purged with argon for 30 min. It was subsequently heated to 80 °C and azobisisobutyronitrile (AIBN) (5.0 mg, 0.031 mmol) dissolved in 0.125 mL of acetonitrile was added. After 8 h of reaction, a yield of 41% telomer was recovered *via* precipitation in cold ethanol (-18 °C), filtered and dried under vacuum.

CmPMMA: ¹H NMR (400 MHz, CDCl₃), δ = 7.5 (d, 1H, H6), 6.8 (d, 1H, H7), 6.7 (s, 1H, H9), 6.1 (s, 1H, H2), 4.0 (t, 2H, H11), 3.6 (t, 2H, H21), 2.4 (s, 3H, H4), 1.8–1.0 (m, 16H + 2n, H12–H20, HP23), 1.2 (m, 3n, HP22).

$M_n = 4300 \text{ g mol}^{-1}$; $M_w = 6235 \text{ g mol}^{-1}$; $D = 1.45$.

Size exclusion chromatography

The SEC equipment was a Varian 390-LC model equipped with a refractometric detector (880 nm). Two PL-gel mix C columns were used at 70 °C using *N,N*-dimethylformamide (DMF) (0.1 wt% LiBr) as eluent at a flow rate of 0.8 mL min⁻¹. A (poly(methyl methacrylate)) PMMA calibration was used to determine the average molar weights using PMMA standards from Agilent. Samples were injected at a concentration of 10 mg mL⁻¹.

Encapsulation of Pheo

2 μL of a 1.23 × 10⁻² M Pheo solution in acetone was added to 0.3 mL of a self-assembly aqueous solution ([CmPOX] = 2.54 × 10⁻³ M). The solution was left standing for one night to evaporate acetone. 1/30 mol/mol Pheo/CmPOX was chosen based on previous experiments.^{8,9}

Dialysis experiments

Solutions of loaded Pheo/self-assemblies were diluted in order to obtain a Pheo concentration of 10⁻⁶ M. 2 mL of these diluted solutions was introduced into a dialysis kit (GE Healthcare Bio-Sciences, membrane with MWCO at 8 kDa) and dialyzed *versus* 800 mL of water at 37 °C. The release of Pheo was followed by measuring the optical density of the internal solution at 688 nm (Pheo alone) and 669 nm (Pheo in self-assemblies). Each dialysis was performed twice. For a comparison, Pheo release was also checked in PBS at 37 °C in the absence of vectors. This did not show any difference in behavior (data not shown), validating the use of pure water for all comparisons.

Dynamic light scattering (DLS)

DLS was carried out at 25 °C on a Malvern (Orsay, France) Zetasizer NanoZS. Solutions were analyzed in triplicate without being filtered in order to characterize the plain samples. Data

were analyzed using the general-purpose non-negative least squares (NNLS) method. The typical accuracy for these measurements was 10–20% for systems exhibiting a polydispersity index lower than 0.4. In the case of cross-linked CmPOX/CmPMMA samples, multiangle dynamic light scattering was performed using an LS Spectrometer (LS instruments) in 3D configuration measuring the scattering from 20° to 150° each 5° or 2°.

All correlograms were analyzed using a custom-made program named STORMS in order to obtain a more precise characterization of the solutions.³⁴ This program has been designed using Matlab and enables the fitting of DLS correlograms using different sets of parameters, corresponding to all hypotheses that have to be made during the treatment. Indeed, going from correlograms to size results implies three levels of hypotheses: the first one consisting of the transformation of autocorrelation data to diffusion coefficients, the second one extracting the size of the scattering object from a diffusion coefficient depending on its geometry, and finally using a model enabling the transformation of the intensity-relative population to a number-relative one. For each step, STORMS provides the choice of different parameters. For the nano-objects presented here, the protocol used a NNLS fitting, assumed a spherical shape for all objects, and the chosen scattering model corresponded to a mixture of micelles and vesicles (maximum micelle size fixed at a radius of 25 nm). Different sets of the range of decay rates and the regularization parameter were used, $\alpha = 2$, range = 2 being the most appropriate one for the samples of this work. Unless stated, this treatment provided residuals lower than 5 × 10⁻³ for all analyses. The polydispersity index (PDI) is the ratio between the variance of the distribution and the square of the mean value of the decay rate, $\bar{\Gamma}$. When the autocorrelation functions were registered at different angles, $\bar{\Gamma}$ obtained is plotted as a function of q^2 in order to obtain the mean diffusion coefficient and, from the Stokes–Einstein equation, the mean hydrodynamic radius according to the equation $\bar{\Gamma} = Dq^2$.

For the evaluation of DMF resistance, similar DLS experiments were performed with increasing quantities of DMF. The position of the measurements was fixed and the refractive index was changed depending on the DMF quantity.

Transmission electron microscopy (TEM)

TEM analyses were performed using a Hitachi HT7700 (Hitachi High Tech, Hitachinaka, Japan) microscope (accelerating voltage of 75 kV). Small amounts of particle suspensions in water were deposited onto a discharged copper grid coated with a carbon membrane, left for 1–3 min depending on the solution, and gently dried with absorbing paper. A drop of uranyl acetate solution was deposited onto the grid for 10 seconds, and the grid was then dried under a lamp for at least 5 min. When the images contained a large number of distinct objects (typically > 200), a measurement of the mean size (as well as the standard deviation) was performed using the ImageJ software (<http://imagej.nih.gov/ij/>).

TEM analyses were also performed one month after the formation of the nanovectors and showed no evolution, proving that either crosslinked or uncrosslinked CmPOX/CmPMMA

vectors were stable for at least one month in pure water at room temperature.

Cryo-electron microscopy (cryo-TEM)

3 μL of sample was deposited onto glow-discharged lacey carbon grids and placed in the thermostatic chamber of a Leica EM-GP automatic plunge freezer, set at 20 $^{\circ}\text{C}$ and 95% humidity. Excess solution was removed by blotting with Whatman no. 1 filter paper for 1–2 seconds, and the grids were immediately flash frozen in liquid ethane at -185°C . The frozen specimens were placed in a Gatan 626 cryo-holder, and cryo TEM was carried out on a Jeol 2100 microscope, equipped with a LaB₆ cathode and operating at 200 kV, under low dose conditions. Images were acquired using the SerialEM software, with a defocus of 1.5–3 μm , on a Gatan US4000 CCD camera. This device was placed at the end of a GIF Quantum energy filter (Gatan, Inc.), and operated in zero-energy-loss mode, with a slit width of 25 eV. Images were recorded at a nominal magnification of 4000 corresponding to calibrated pixel sizes of 1.71 \AA .

Cell culture

The HCT-116 cell line (ATCC #CCL-247) originated from a human colorectal carcinoma. HCT-116 cells were grown in Dulbecco's Modified Eagles Medium (Invitrogen) containing glucose (4.5 g L^{-1}), GlutaMAX and pyruvate, supplemented with 10% (v/v) heat inactivated fetal bovine serum (FBS), 100 U mL^{-1} penicillin and 100 $\mu\text{g mL}^{-1}$ streptomycin. Cells were maintained at 37 $^{\circ}\text{C}$ in a humidified atmosphere containing 5% CO_2 .

Cytotoxicity and phototoxicity of Pheo-loaded polymeric nanovectors

These biological tests were performed on 2D adherent cell monolayers. HCT-116 tumor cells were seeded in 96-well plates (4000 cells per well) 24 h prior to experiment. Cytotoxicity of polymer self-assemblies was assessed after 24 h of cell incubation with nanovectors at a CmPOX polymer concentration of 30 μM . To assess the phototoxicity of nanovectors in a photodynamic therapy context, cells were incubated for 30 min at 37 $^{\circ}\text{C}$ with Pheo-loaded self-assemblies (1/30 mol/mol) (*i.e.*, 1 μM pheophorbide). Then, cells underwent a set of two photoactivations,⁸ which were performed using an overhead projector with a band-pass filter ($\lambda > 400 \text{ nm}$), representing a total dose of 12 J cm^{-2} . In brief, cells were illuminated for 2 min, followed by a break for 2 min, and once again 2 min of illumination. The concentration used for Pheo alone was 1 μM corresponding to the same concentration as in the experiments with the loaded polymer self-assemblies. Viability was assessed using a metabolic test based on PrestoBlue reagent (Invitrogen) according to the manufacturer's instructions. For every set of experiments carried out three times independently, six biological replicates were produced and analyzed. Statistical differences between values were assessed by one-way ANOVA followed by a Dunnett's multiple comparisons test, which compares each condition with the control condition. All data were expressed as mean \pm standard error of the mean (SEM), and overall statistical significance was set at $p < 0.05$. A set of PDT experiments

was carried out independently two times using 0.1 and 0.5 μM Pheo-loaded nanovectors.

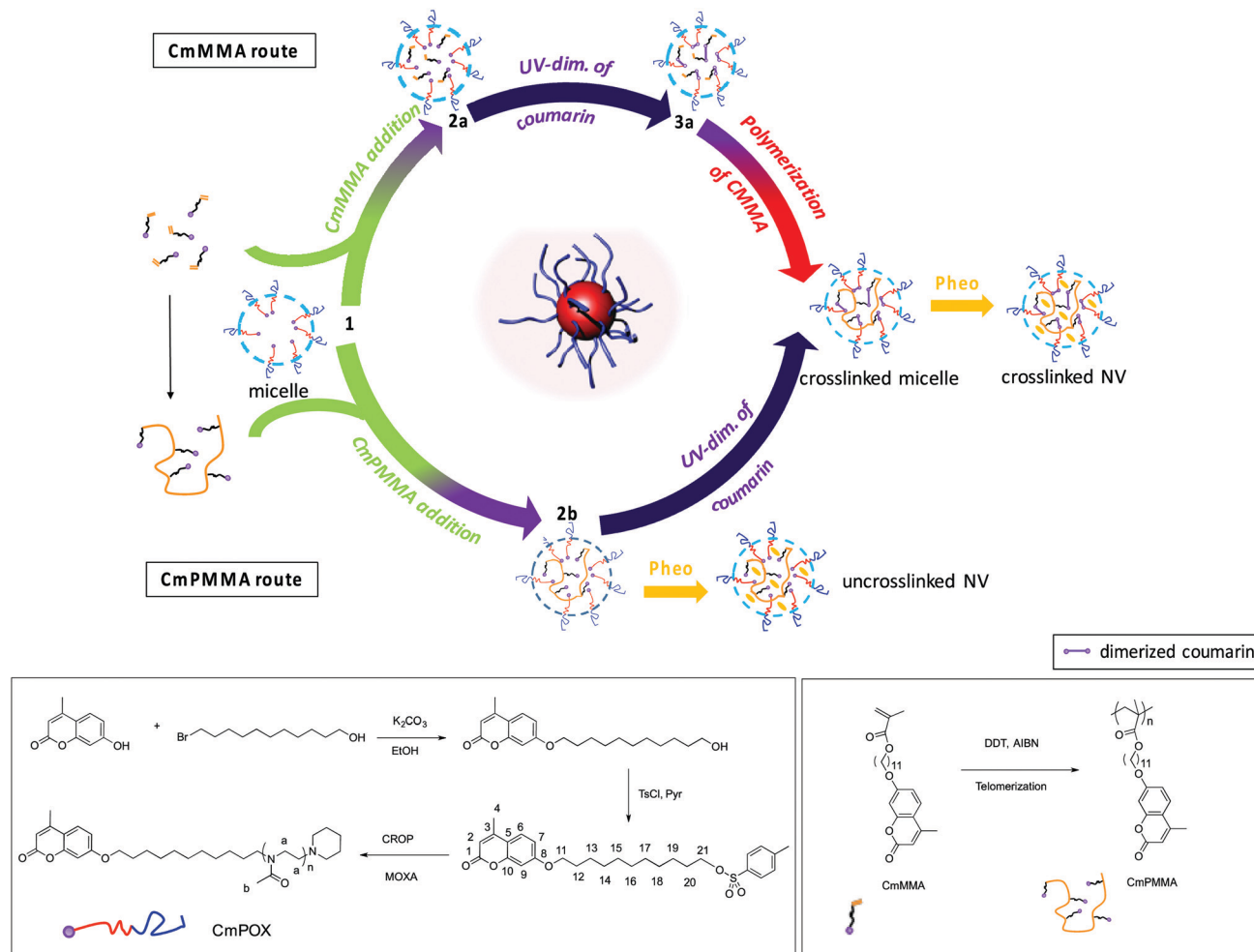
Results

In order to obtain a polymer micelle, poly(2-methyl-2-oxazoline) (POX) was employed as a hydrophilic stabilizing external block. The hydrophobic core was composed of a C11 alkyl chain to help the self-assembling process, both connected to the POX block and a photo-reactive group such as coumarin, well-known to dimerize under UV irradiation, as already published³¹ (Fig. S1, ESI[†]). This linear amphiphilic polymer (CmPOX) is only able to photo-link two by two the tangled chains but not crosslink the micelle core as previously discussed in a comparison to grafted amphiphilic copolymers.³⁵ To ensure the stabilization of the micelle by crosslinking, coumarin-functionalized methyl methacrylate (CmMMA)³⁶ was added (Scheme 1, step 2a) since it was able to react by photo-dimerization both with its own coumarin unit as well as that of CmPOX (Scheme 1, step 3a) and photo-polymerization of the methacrylate unit.

CmPOX was directly dispersed in water and small 13 nm polymer micelles were observed *via* cryo-TEM (Scheme 1, step 1, Fig. S10, ESI[†]), which was consistent with earlier results.³⁶ CmMMA was then encapsulated into the formed micelles by the addition of a small volume of CmMMA acetone solution (Scheme 1, step 2a). A CmMMA/CmPOX ratio of 7 mol% (1 wt%) was chosen to avoid any destabilization of the micelles. This was checked using TEM images, and they showed that no modification was present even after subsequent coumarin dimerization and CmMMA radical polymerization (Fig. S6, ESI[†]). The monitoring of the polymerization *via* ^1H NMR spectroscopy (Fig. S7, ESI[†]) showed an incomplete polymerization leading to the presence of residual monomer. Since its uncontrolled release could have been detrimental for the PDT application, this path was abandoned.

In order to avoid residual CmMMA in the self-assemblies, this monomer was first polymerized before encapsulating into the CmPOX micelles (Scheme 1, CmPMMA route). Telomerization was performed using dodecanethiol as a transfer agent and AIBN as a radical initiator following well-known procedures.³⁷ The resulting CmPMMA oligomers were characterized by ^1H NMR and size exclusion chromatography (Fig. S8 and S9, ESI[†]) and exhibited a molar mass close to 4000 g mol^{-1} . Their encapsulation in CmPOX micelles was similarly performed through the CmMMA route using a small acetone solution volume on preformed CmPOX micelles (Scheme 1, step 2b). In this system, the amount of encapsulated CmPMMA was 13 wt%, and TEM results showed the presence of the same type of micelles compared to CmPOX alone or CmPOX/CmMMA (Fig. S10, ESI[†]).

The mixed micelles were then irradiated at 360 nm to crosslink their hydrophobic core by cross- and sym-dimerization between coumarin units of CmPOX and CmPMMA. TEM analyses showed small micelles of CmPOX close to 10 nm, which did not change with the addition of CmPMMA and upon the irradiation and the loading of Pheo (Fig. 1). It is noteworthy that TEM images of Pheo-loaded nanovectors were very different from Pheo dispersed in



Scheme 1 Principle of formation of photo-crosslinked micelles.

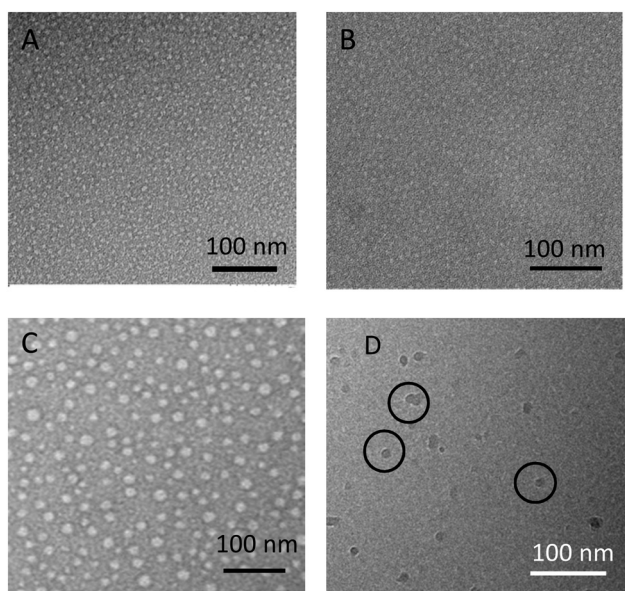


Fig. 1 TEM images of CmPOX/CmPMMA micelles: uncrosslinked (A), crosslinked (B) and crosslinked and loaded with Pheo (C). Cryo-TEM images of crosslinked CmPOX/CmPMMA micelles loaded in Pheo, circles indicate the presence of the objects (D).

water (Fig. S11, ESI[†]). Cryo-TEM characterization confirmed the presence of small micelles exhibiting a size between 13 and 26 nm (Fig. 1). Although TEM and cryo-TEM enabled us to visualize the self-assemblies, they both have well-known limitations. TEM requires drying of the sample, which might lead to a re-organization, while cryo-TEM can enrich the solution in small objects owing to the very thin ice thickness. Furthermore, they both provide the analysis of only several hundreds of objects at most, which might not reflect the overall sample solution.

Therefore, the second typical characterization method of self-assembly size is mono-angle Dynamic Light Scattering (DLS), which enables the batch analysis of the solution. The intensity-average analysis showed the presence of large objects, with a first population close to 300 nm and a second one exhibiting a size above 600 nm (Fig. 2 and Fig. S12, ESI[†]). On the other hand, the number average analysis pointed to the majority presence of small micelles with a size lower than 50 nm. However, the presence of large objects impeded any detailed characterization of this population. This result can be explained taking into account the scattered light intensity dependency with the size of the scattering object. Since this is linked to R^6 , it is well known that the presence of even a small

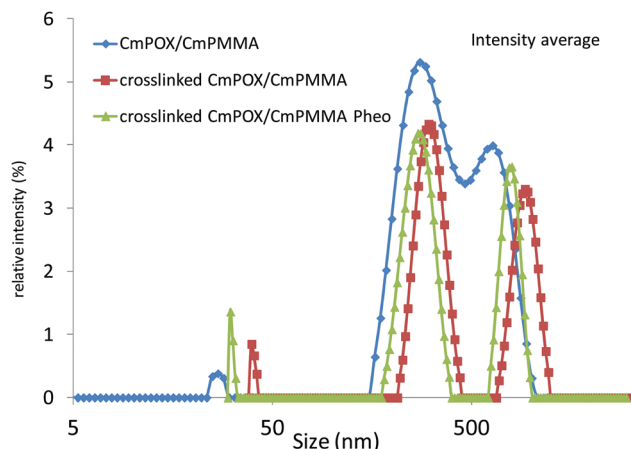


Fig. 2 Intensity-average DLS of CmPOX/CmPMMA self-assemblies.

amount of large objects will hinder the DLS detection of small ones.³⁴ This can be considered as an extreme case where the difference of small *versus* large self-assemblies is too large to properly extract the exact size of the micelles by DLS. However, DLS pointed to the presence of large objects. These were indeed observed *via* TEM, but on very few images (Fig. S13, ESI†).

In order to analyze more thoroughly the sample solutions, further characterization was carried out by multi-angle DLS in the case of crosslinked CmPOX/CmPMMA (Fig. S14 and S15, ESI†). The direct analysis of the solution yielded the same result as that with the mono-angle DLS characterization, *i.e.* the presence of large objects with a size close to 280 nm in good agreement with the smaller population observed at 173° (see DLS Int in Table 1). It is noteworthy that these analyses were performed upon dilution of the samples and that no population at *ca.* 950 nm was observed in contrast to mono-angle DLS. This points to the hypothesis that this 950 nm population is composed of self-assembly aggregates that were destroyed by dilution. Filtration of the solution at 0.2 μm was performed

in order to eliminate the large objects and allow a better estimation of the size of the smaller self-assemblies. This led to the appearance of 2 populations below 100 nm, the first one close to 90 nm and the second one around 6 nm in accordance with the more abundant population observed *via* TEM. Comparing the scattered intensity before and after filtration indicated that the small population concentrations were at least 30 times higher than the 280 nm objects.

Regarding the overall characterization of these self-assemblies, this is an extreme case illustrating the importance of multiple analyses of polymer self-assemblies. Based on Table 1, the main conclusions are that the majority of self-assemblies exhibit a size below 40 nm whereas the minority has a size above 200 nm. The quantification of each population and their further characterization will imply the use of separation techniques such as Flow Field Flow Fractionation, as well as other scattering techniques such as X-ray or neutron scattering. This was however beyond the scope of this study.

As already discussed, the development of crosslinked polymeric vectors aims at increasing their stability. It is therefore important to examine the resistance of such objects under challenging conditions. Before exposing them to biological media, a useful test is to assess their resistance towards a solvent that is able to dissolve the copolymers. For this, uncrosslinked and crosslinked CmPOX/CmPMMA solutions were diluted with increasing amounts of DMF and characterized by mono-angle DLS (Table 2).

Since we formerly discussed the problem of evaluating the size of the objects by DLS, we only focused on the scattered light intensity (as evaluated using the Derived Count Rate, DCR). This is another relevant factor to assess, because presenting only the value of the size obtained by DLS might be misleading (a mixture of 95 wt% free disintegrated polymer/5 wt% nano-objects would exhibit the same un-modified DLS result compared to the pure nano-object). The experimental DCR was compared to the theoretical minimum one, obtained by a simple decrease of the intensity owing to dilution, therefore not taking into

Table 1 Characterization of polymer self-assemblies

Technique	CmPOX	CmPOX/CmPMMA	Crosslinked CmPOX/CmPMMA	CmPOX/CmPMMA/Pheo	Crosslinked CmPOX/CmPMMA/Pheo
DLS Int	— ^a	280/612	320/950	— ^a	278/780
DLS Num		244	41		32
TEM		9 ± 2	8 ± 2	n.d.	11 ± 2
Cryo-TEM	13.2 ± 2.5	n.d.	n.d.	15.9 ± 2.5 ^b	12.7 ± 3.5

^a DLS data not reliable enough for treatment. ^b Number of objects measured <30.

Table 2 Swelling tests in DMF with various CmPOX/CmPMMA micelles monitored by scattered intensity

	0% DMF	20 vol%	40 vol%	60 vol%
Crosslinked CmPOX/CmPMMA DCRexp	49 000	41 700	24 700	10 300
DCRth		39 200	29 400	19 600
DCRexp/DCRth		1.10	0.84	0.53
Uncrosslinked CmPOX/CmPMMA DCRexp	51 800	26 700	10 900	4700
DCR th		41 400	31 100	20 700
DCRexp/DCRth		0.64	0.35	0.23

account possible swelling due to the presence of the good solvent. Any strong decrease compared to this theoretical DCR should be a sign of self-assembly disintegration owing to dissolution. In such tests, uncrosslinked systems are expected to resist only poorly to the addition of a good solvent, whereas crosslinked ones should possibly swell without disintegrating. Table 2 shows that it is indeed the case, with the uncrosslinked system beginning to dissociate at 20 vol% DMF, whereas the crosslinked one holds up to 40 vol%. This result is very comparable to other studies presenting the scattered intensity.^{38,39} Soft nano-objects like these polymeric micelles, although crosslinked, remain breakable under harsh conditions such as their exposure to good solvents. In fact, among all crosslinked polymeric micelles described in the literature, only one example has been shown to exhibit an ideal behavior, remaining completely stable upon organic solvent addition.⁴⁰

The characterization of the self-assemblies *via* TEM proved that Pheo was very probably inside the polymer micelles and that loading did not modify their size. Further proof was given by UV-visible absorption spectra, particularly zooming on the 600–700 nm area. Indeed, it is well-known that Pheo absorbance is sensitive to its environment. Under aqueous conditions, the band of this zone exhibits a maximum at 690 nm (Fig. 3). In the presence of crosslinked CmPOX/CmPMMA micelles, this band was shifted to 670 nm, which is characteristic of a more hydrophobic environment⁷ such as the micelle core composed of alkyl chains decorated by coumarin dyes.

Before assessing cytotoxicity and PDT efficiency of these polymeric nanovectors, a last physico-chemical characterization consisted of examining the kinetics of Pheo release in simple dialysis models, as illustrated in Fig. 4. The results show that Pheo was released more slowly in crosslinked nanovectors compared to the uncrosslinked ones. For uncrosslinked vectors, Pheo was released in a similar manner to Pheo alone (in the absence of any vector) at the beginning of the dialysis.

After physico-chemical characterization of these nanovectors, we moved to biological tests. Three independent *in vitro* experiments

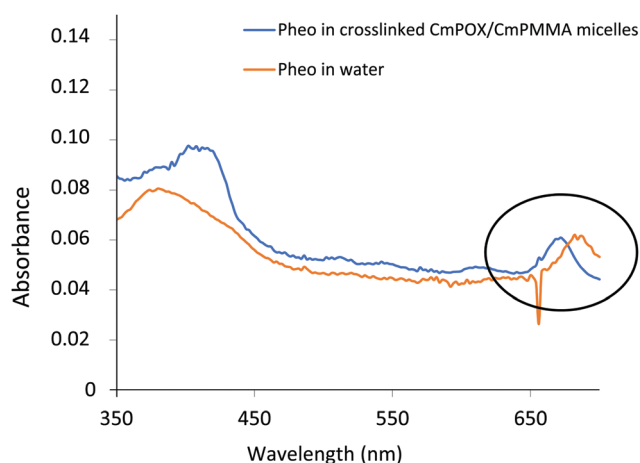


Fig. 3 UV-visible absorption of Pheo in water or in CmPOX/CmPMMA crosslinked systems.

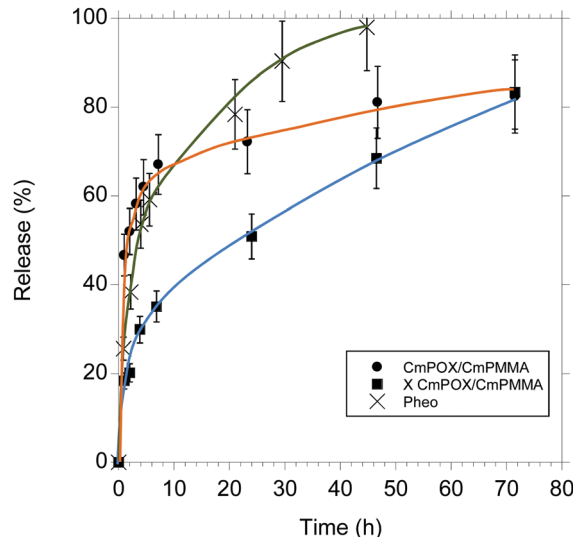


Fig. 4 Pheo release follow-up by dialysis ([Pheo] = 10^{-6} M, 37 °C, in pure water).

on human colorectal cancer cells HCT-116 showed that no significant cell viability decrease was observed after 24 h of incubation with the first generation of micelles based on CmPOX or CmPMMA alone (Fig. 5A). However, it has to be noted that micelles bearing in their core CmPMMA statistically decrease cell viability under uncrosslinked conditions and tend to decrease cell viability under crosslinked conditions (86.6% and 89.2%, respectively). It is noteworthy that Pheo alone is known to be non cytotoxic without any irradiation at the same concentration.^{8,9,34}

PDT experiments were carried out *in vitro* on human tumor cells HCT-116 to assess the potential of these nanovectors loaded with or without 1 μ M Pheo for photodynamic therapy, as summarized in Fig. 5B. Non-Pheo loaded CmPOX, CmPMMA, un-crosslinked (CmPOX/CmPMMA) and crosslinked (X CmPOX/CmPMMA) nanovectors did not alter cell viability. At this 1 μ M concentration, Pheo alone statistically reduced cell viability by approximately 7%, which was consistent with already published results.⁹ Interestingly, when this photosensitizer was encapsulated in un-crosslinked or crosslinked nanovectors, cell viability dramatically decreased to only 30%. This means that nanovectors were highly efficient to deliver Pheophorbide a to tumor cells. It has to be noted that the difference observed between uncrosslinked and crosslinked nanovectors was not statistically significant, which means that crosslinking did not cause a supplementary beneficial effect of the nanovectors in terms of photodynamic therapy in this monolayer cell culture. Other PDT experiments were carried out with a lower pheophorbide a concentration (*i.e.*, 0.1 μ M and 0.5 μ M) (Fig. S16, ESI[†]). A dose effect was observed: when encapsulated in un-crosslinked (CmPOX/CmPMMA) and cross-linked (X CmPOX/CmPMMA) nanovectors, cell viability was quantified around 65% with 0.1 μ M Pheo-loaded nanovectors and 30% with 0.5 μ M Pheo-loaded nanovectors. Interestingly, under these conditions, pheophorbide alone was not concentrated enough to induce a loss of cell viability, indicating a high benefit of encapsulating it within nanovectors.

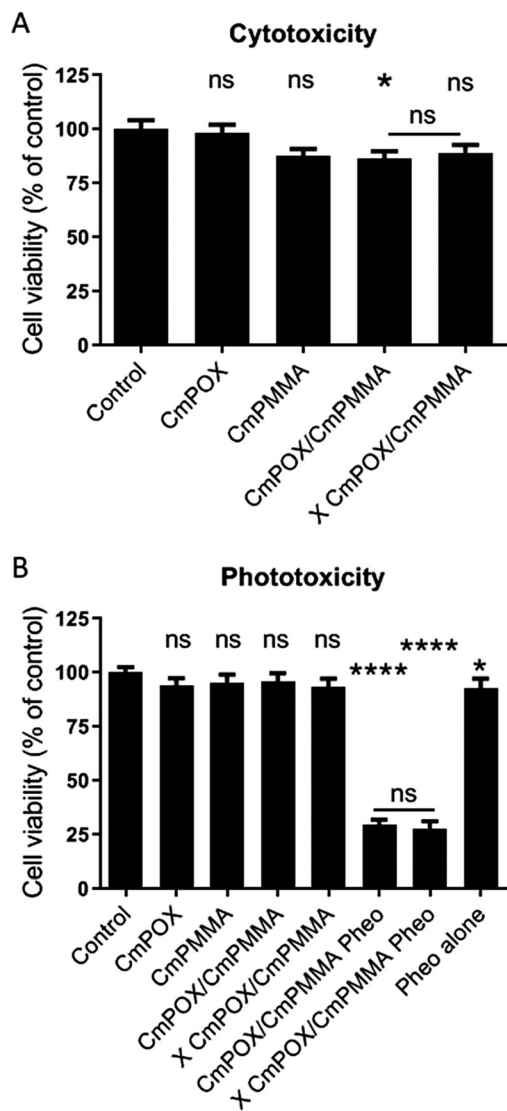


Fig. 5 Cytotoxicity and phototoxicity of (un)crosslinked polymeric nanovectors (CmPOX/CmPMMA) on human tumor cells HCT-116. (A) Cytotoxicity was quantified through the metabolic test using PrestoBlue after 24 h of incubation with (un)crosslinked polymeric nanovectors CmPOX/CmPMMA. (B) Effect of 1 μ M Pheo-loaded nanovectors on cell viability after using the photodynamic therapy protocol assessed with the metabolic test with PrestoBlue 24 h after treatment. X: crosslinked nanovectors; Pheo: pheophorbide a. Statistical analysis was done by using one-way ANOVA followed by a Dunnett's multiple comparisons test on 18 independent biological replicates comparing each condition with the control one. Statistical significance was compared between Pheo-loaded cross-linked and non-crosslinked nanovectors using *t*-test. p value $< 0.05 = *$; $p < 0.0001 = ****$; ns = non-significant.

Discussion

The ideal nanovector should exhibit numerous properties, such as adequate size to benefit from the EPR effect, surface zeta potential close to neutrality, biocompatibility, and the ability to deliver its cargo at an appropriate rate depending on the application. To optimize the vectors and get closer to this difficult goal, several leads have been examined in the literature,

one of these being crosslinking the vector, increasing its intrinsic stability and therefore its mean blood circulation time. The same increase of stability has also been observed in the vector presented here, since its resistance to swelling in DMF has been improved substantially, as shown by the scattered light intensity that did not drop drastically before 60 vol% DMF.

Developing polymeric nanovectors implies thorough characterization of the self-assemblies, which can often be tricky, owing to the possible presence of multi-populations. The nanovector presented here is a typical difficult case. Indeed, both TEM and cryo-TEM indicated the presence of small nano-objects below 20 nm, whereas the classically used intensity-average DLS analysis gave results ranging from 200 nm to 1 μ m. This discrepancy can be explained by the intrinsic weakness of DLS in analyzing multi-population systems, as we clearly showed in a previous study.³⁴ Using multi-angle static/dynamic light scattering proved unsuccessful in resolving this situation. Nanoparticle Tracking Analysis (NTA) is another technique often used to characterize vesicles, providing both their size and the distribution of different populations. NTA was used for the system developed here (data not shown), but, unsurprisingly, only the large population was once again observed, since NTA is known for its lower size limit, close to 50 nm for soft matter. Another possible technique is Flow Field Flow Fractionation (F-FFF), providing a separation of the nano-objects by their size before analysis by light scattering detectors. We have previously shown that this technique is particularly relevant for the characterization of nanovectors, such as poly(ethylene oxide-*b*- ϵ -caprolactone).^{41,42} Tentative analysis of the present samples was performed, but led to unreproducible results, possibly owing to the responsiveness of the vectors to the shear in the F-FFF cell, however small. Developing an appropriate method to characterize CmPOX self-assemblies was beyond the scope of this work, but should be performed before any *in vivo* injection, to get a precise knowledge of the vector solution content.

Coumarin was chosen in the process for its ability to dimerize under UV irradiation, enabling crosslinking of the constructions. However, the coumarin ring system is well known to display multiple *in vitro*, *in vivo* and *ex vivo* pharmacological effects such as antimetabolic, anticancer and cytotoxic effects.^{43,44} For this purpose, we analyzed the nanovector cytotoxic effect on human tumor colorectal cancer cells HCT-116. Interestingly, once integrated in the nanovectors, coumarin did not interfere with cell viability (CmPOX or CmPMMA) but when combined in CmPOX/CmPMMA nanovectors presenting a higher concentration of coumarin, a slight trend was observed in decreasing cell viability. This property is interesting because it reinforces the anticancer potential of the nanovectors designed in this study for photodynamic therapy. In the literature, only a few cases of polymeric self-assemblies crosslinked through coumarin dimerization have been described. One example was from our team using different polyoxazoline polymers.^{31,35,45} This was focused on the physical chemistry aspect, in order to better understand how the microstructure of the polymer could interfere with the stability of the self-assemblies. Two other studies described coumarin-crosslinked polymeric nanovectors for the release of doxorubicin,^{46,47} either

for a light-induced release or as a simple photo-crosslinkable system. Owing to the already mentioned biological properties of coumarin, such studies have to be controlled so that coumarin behavior is unambiguous. In the case of this study, the biological tests prove that the main response comes from the PDT effect arising from Pheo.

We also showed that polymeric self-assemblies, both un-crosslinked and crosslinked, drastically decreased tumor cell viability after photo-activation. These results are comparable with other systems previously described by our group.^{7,8} We previously demonstrated using poly(ethylene oxide-*b*- ϵ -caprolactone) systems in 2D cell cultures that crosslinked and un-crosslinked vectors were efficient in reducing cell viability.⁹ In the literature, crosslinking of the nanovectors is most often performed to optimize *in vivo* resistance. Therapeutic efficiency is not systematically improved, and one should be very careful in commenting on 2D *in vitro* results. Indeed, examples have shown that in some cases, crosslinked vectors are less efficient compared to free drugs *in vitro* but this is reversed *in vivo*.^{48–50} Avoiding systematic *in vivo* experiments is important for ethics, and this is the reason why *in vitro* 3D cell models have increasingly been developed. Thus, in our earlier study,⁹ we also showed in a 3D tumor model named spheroid that the crosslinked vectors presented higher antitumor activity than un-crosslinked ones. Such a behavior was also observed by Stenzel using vectorized paclitaxel.^{51,52} A way to go beyond deciphering potential in photodynamic therapy would be to analyze the interactions and efficiency of these nanoparticles with tumor and normal cells grown in a 3D tissue model such as spheroids.

Finally, comparing our results with those obtained on poly(2-ethyl-oxazoline-*b*-D,L-lactide) as put forth by Lai shows close results. Lai determined an IC₅₀ for their photosensitizer close to 1.5 μ M whereas that of our system is between 0.1 and 0.5 μ M. However, one should be very careful while making comparisons using PDT, since the cell lines are different, along with the exact protocol of photosensitizer irradiation (power, duration...). A strong difference is, however, that contrary to them, we observe a strong improvement in the *in vitro* PDT treatment by encapsulation of the chosen photosensitizer, underlining the importance of the design of the nanovector.

Conclusion

The efficiency of poly(2-methyl-2-oxazoline) self-assemblies as a potential Pheophorbide a carrier for photodynamic therapy was demonstrated. Pheo has undeniably been encapsulated in the self-assemblies, increasing its photocytotoxicity. Consequently, POX polymers constitute a powerful platform for further development of nanovectors. The introduction of a controlled and limited aliphatic chain and the photoreactive coumarin units provides parameters to tune finely the vectors. Further work will be performed in order to adapt the vector to *in vivo* conditions.

Conflicts of interest

There are no conflicts to declare.

Notes and references

- V. Weissig and D. Guzman-Villanueva, *Int. J. Nanomed.*, 2015, **10**, 1245–1257.
- Z. Tang, C. He, H. Tian, J. Ding, B. S. Hsiao, B. Chu and X. Chen, *Prog. Polym. Sci.*, 2016, **60**, 86–128.
- A. Varela-Moreira, Y. Shi, M. H. A. M. Fens, T. Lammers, W. E. Hennink and R. M. Schiffelers, *Mater. Chem. Front.*, 2017, **1**, 1485–1501.
- Y. Matsumura and H. Maeda, *Cancer Res.*, 1986, **46**, 6387–6392.
- H. Maeda, *Bioconjugate Chem.*, 2010, **21**, 797–802.
- S. S. Lucky, K. C. Soo and Y. Zhang, *Chem. Rev.*, 2015, **115**, 1990–2042.
- K. Knop, A.-F. Mingotaud, N. El-Akra, F. Violleau and J.-P. Souchard, *Photochem. Photobiol. Sci.*, 2009, **8**, 396–404.
- L. Gibot, A. Lemelle, U. Till, B. Moukarzel, A. F. Mingotaud, V. Pimienta, P. Saint-Aguet, M. P. Rols, M. Gaucher, F. Violleau, C. Chassenieux and P. Vicendo, *Biomacromolecules*, 2014, **15**, 1443–1455.
- U. Till, L. Gibot, P. Vicendo, M. P. Rols, G. Gaucher, F. Violleau and A. F. Mingotaud, *RSC Adv.*, 2016, **6**, 69984–69998.
- S. Wang, F. Yuan, K. Chen, G. Chen, K. Tu, H. Wang and L.-Q. Wang, *Biomacromolecules*, 2015, **16**, 2693–2700.
- H. Hu, X. Yan, H. Wang, J. Tanaka, M. Wang, W. You and Z. Li, *J. Mater. Chem. B*, 2019, **7**, 1116–1123.
- Y. Han, Z. Chen, H. Zhao, Z. Zha, W. Ke, Y. Wang and Z. Ge, *J. Controlled Release*, 2018, **284**, 15–25.
- Y. Wang, G. Wei, X. Zhang, F. Xu, X. Xiong and S. Zhou, *Adv. Mater.*, 2017, **29**, 1605357.
- X. Wei, L. Liu, X. Guo, Y. Wang, J. Zhao and S. Zhou, *ACS Appl. Mater. Interfaces*, 2018, **10**, 17672–17684.
- X. Wang, J. Wang, J. Li, H. Huang, X. Sun and Y. Lv, *J. Drug Delivery Sci. Technol.*, 2018, **48**, 414–421.
- K. Knop, R. Hoogenboom, D. Fischer and U. S. Schubert, *Angew. Chem., Int. Ed.*, 2010, **49**, 6288–6308.
- H. Schellekens, W. E. Hennink and V. Brinks, *Pharm. Res.*, 2013, **30**, 1729–1734.
- Q. Yang and S. K. Lai, *Wiley Interdiscip. Rev.: Nanomed. Nanobiotechnol.*, 2015, **7**, 655–677.
- A. S. Abu Lila, H. Kiwada and T. Ishida, *J. Controlled Release*, 2013, **172**, 38–47.
- O. Sedlacek, B. D. Monnery, S. K. Filippov, R. Hoogenboom and M. Hruby, *Macromol. Rapid Commun.*, 2012, **33**, 1648–1662.
- T. Lorson, M. M. Lübtow, E. Wegener, M. S. Haider, S. Borova, D. Nahm, R. Jordan, M. Sokolski-Papkov, A. V. Kabanov and R. Luxenhofer, *Biomaterials*, 2018, **178**, 204–280.
- T. R. Dargaville, J.-R. Park and R. Hoogenboom, *Macromol. Biosci.*, 2018, **18**, 1800070.
- P. H. Kierstead, H. Okochi, V. J. Venditto, T. C. Chuong, S. Kivimae, J. M. J. Fréchet and F. C. Szoka, *J. Controlled Release*, 2015, **213**, 1–9.
- R. W. Moreadith, T. X. Viegas, M. D. Bentley, J. M. Harris, Z. Fang, K. Yoon, B. Dizman, R. Weimer, B. P. Rae, X. Li, C. Rader, D. Standaert and W. Olanow, *Eur. Polym. J.*, 2017, **88**, 524–552.
- Y. Li, M. Vergaelen, E. Schoolaert, R. Hoogenboom and K. De Clerck, *Eur. Polym. J.*, 2019, **112**, 24–30.

- 26 Y. Li, M. Vergaelen, X. Pan, F. E. Du Prez, R. Hoogenboom and K. De Clerck, *Macromolecules*, 2018, **51**, 6149–6156.
- 27 P. Šrámková, A. Zahoranová, Z. Kroneková, A. Šišková and J. Kronek, *J. Polym. Res.*, 2017, **24**, 82.
- 28 Y. Chujo, K. Sada and T. Saegusa, *Macromolecules*, 1990, **23**, 2693–2697.
- 29 Y. Imai, K. Naka and Y. Chujo, *Polym. J.*, 1998, **30**, 990–995.
- 30 M.-J. Shieh, C.-L. Peng, W.-L. Chiang, C.-H. Wang, C.-Y. Hsu, S.-J. J. Wang and P.-S. Lai, *Mol. Pharmaceutics*, 2010, **7**, 1244–1253.
- 31 L. Korchia, C. Bouilhac, V. Lapinte, C. Travelet, R. Borsali and J.-J. Robin, *Polym. Chem.*, 2015, **6**, 6029–6039.
- 32 S. Emami and S. Dadashpour, *Eur. J. Med. Chem.*, 2015, **102**, 611–630.
- 33 L. Aoife, *Curr. Pharm. Des.*, 2004, **10**, 3797–3811.
- 34 U. Till, L. Gibot, C. Mingotaud, P. Vicendo, M. P. Rols, M. Gaucher, F. Violleau and A. F. Mingotaud, *Nanotechnology*, 2016, **27**, 315102.
- 35 L. Korchia, V. Lapinte, C. Travelet, R. Borsali, J.-J. Robin and C. Bouilhac, *Soft Matter*, 2017, **13**, 4507–4519.
- 36 D. Rayeroux, C. Travelet, V. Lapinte, R. Borsali, J.-J. Robin and C. Bouilhac, *Polym. Chem.*, 2017, **8**, 4246–4263.
- 37 B. Boutevin and Y. Pietrasanta, *Comprehensive Polymer Science*, Pergamon Press, New York, 1989, vol. 3, pp. 185–194.
- 38 K. Wang, Y. Liu, W.-J. Yi, C. Li, Y.-Y. Li, R.-X. Zhuo and X.-Z. Zhang, *Soft Matter*, 2013, **9**, 692–699.
- 39 Y.-C. Wang, Y. Li, T.-M. Sun, M.-H. Xiong, J. Wu, Y.-Y. Yang and J. Wang, *Macromol. Rapid Commun.*, 2010, **31**, 1201–1206.
- 40 Y. Han, J. Li, M. Zan, S. Luo, Z. Ge and S. Liu, *Polym. Chem.*, 2014, **5**, 3707–3718.
- 41 J. Ehrhart, A.-F. Mingotaud and F. Violleau, *J. Chromatogr. A*, 2011, **1218**, 4249–4256.
- 42 U. Till, M. Gaucher-Delmas, P. Saint-Aguet, G. Hamon, J.-D. Marty, C. Chassenieux, B. Payré, D. Goudounèche, A. F. Mingotaud and F. Violleau, *Anal. Bioanal. Chem.*, 2014, **406**, 7841–7853.
- 43 P. Xin-Mei, L. V. D. Guri and Z. Cheng-He, *Curr. Pharm. Des.*, 2013, **19**, 3884–3930.
- 44 S. Devulapally, G. Chandraiah and D. Pramod Kumar, *Mini-Rev. Med. Chem.*, 2018, **18**, 113–141.
- 45 L. Korchia, C. Bouilhac, A. Aubert, J. J. Robin and V. Lapinte, *RSC Adv.*, 2017, **7**, 42690–42698.
- 46 X. Zhang, Y. Wang, G. Li, Z. Liu, Z. Liu and J. Jiang, *Macromol. Rapid Commun.*, 2017, **38**, 1600543.
- 47 H. He, Y. Ren, Y. Dou, T. Ding, X. Fang, Y. Xu, H. Xu, W. Zhang and Z. Xie, *RSC Adv.*, 2015, **5**, 105880.
- 48 R. Yang, F. Meng, S. Ma, F. Huang, H. Liu and Z. Zhong, *Biomacromolecules*, 2011, **12**, 3047–3055.
- 49 Y. Shi, R. van der Meel, B. Theek, E. Oude Blenke, E. H. E. Pieters, M. H. A. M. Fens, J. Ehling, R. M. Schiffelers, G. Storm, C. F. van Nostrum, T. Lammers and W. E. Hennink, *ACS Nano*, 2015, **9**, 3740–3752.
- 50 M. Taleli, M. Iman, A. K. Varkouhi, C. J. F. Rijcken, R. M. Schiffelers, T. Etrych, K. Ulbrich, C. F. van Nostrum, T. Lammers, G. Storm and W. E. Henninck, *Biomaterials*, 2010, **31**, 7797–7804.
- 51 A. W. Du, H. Lu and M. H. Stenzel, *Biomacromolecules*, 2015, **16**, 1470–1479.
- 52 H. Lu, R. H. Utama, U. Kitiyotsawat, K. Babiuch, Y. Jiang and M. H. Stenzel, *Biomater. Sci.*, 2015, **3**, 1085–1095.